Aggregation studies of the water-soluble gadofullerene magnetic resonance imaging contrast agent: [Gd@C82O6(OH)(16)(NHCH2CH2COOH)(8)](x)

ARTICLE *in* THE JOURNAL OF PHYSICAL CHEMISTRY B · SEPTEMBER 2006

Impact Factor: 3.3 · DOI: 10.1021/jp0615609 · Source: PubMed

7 AUTHORS, INCLUDING:

Chunying Shu
Chinese Academy of Sciences
98 PUBLICATIONS **1,955** CITATIONS
SEE PROFILE

Jun-Feng Xiang
Chinese Academy of Sciences
185 PUBLICATIONS **2,882** CITATIONS
SEE PROFILE

Chun-Ru Wang
Chinese Academy of Sciences
66 PUBLICATIONS **2,138** CITATIONS
SEE PROFILE

Aggregation Studies of the Water-Soluble Gadofullerene Magnetic Resonance Imaging Contrast Agent: $[Gd@C_{82}O_6(OH)_{16}(NHCH_2CH_2COOH)_8]_x$

Chun-Ying Shu,[†] Er-Yun Zhang,[†] Jun-Feng Xiang,[†] Chuan-Feng Zhu,[†] Chun-Ru Wang,*[,†] Xin-Long Pei,[‡] and Hong-Bin Han[‡]

Beijing National Laboratory for Molecular Sciences, Institute of Chemistry, Chinese Academy of Sciences, Beijing 100080, China, and Radiology Department of the Third Hospital, Peking University, Beijing 100083, China

Received: March 14, 2006; In Final Form: June 16, 2006

The aggregation behavior of the newly synthesized gadofullerene magnetic resonance imaging (MRI) contrast agent, i.e., $Gd@C_{82}O_6(OH)_{16}(NHCH_2CH_2COOH)_8$ (abbreviated as AAD-EMF), was studied in detail by dynamic light scattering, scanning electron microscopy, T_1-weighted magnetic resonance, and atomic force microscopy. It was revealed that the AAD-EMF aggregation in aqueous solution is pH-dependent. At pH 2, the AAD-EMF first self-assemble to form ca. 30 nm small clusters, and then dozens of the small clusters further aggregate to form large grapelike particles. At pH 7, the aggregates are also ca. 30 nm small clusters, but they are hard to further aggregate except for forming some cluster dimers or trimers, so AAD-EMF aggregates have a narrow size distribution by this time. At pH 9, the AAD-EMF aggregations cover a large range of continuous hydrodynamic diameters from 30 to 2000 nm. On the basis of the above observations, the aggregating mechanism of AAD-EMF under different pH values was proposed by concurrently considering the hydrogen-bonding effect and the dipolar interactions between AAD-EMF.

1. Introduction

Endohedral metallofullerenes[1] (hereafter abbreviated as EMFs) are constructed by fullerene encapsulating one or more metal atoms. Due to the involvement of metal atoms inside the molecule, most EMFs exhibit metallic properties, and some monometallic EMFs even behave like "superatoms" of the corresponding encaged metals.[2] In fact, it is the special structure and novel properties of EMFs that lead to their potential applications[3−9] in various fields such as chemistry, physics, electronics, medicine, and biological science.

Gadolinium has a half-filled f-orbital shell that exhibits strong paramagnetic properties, so some gadolinium chelate complexes, e.g., Gd−DTPA, Gd−DO3A, Gd−DOTA, etc., have been broadly applied as commercial magnetic resonance imaging (MRI) contrast agents[10,11] in the clinic. However, recent studies revealed that the Gd-based EMFs also display the strong paramagnetic properties of Gd^{3+},[12] and the water-soluble gadolinium-based EMFs,[7−9,13,14] e.g., $Gd@C_{82}(OH)_x$,[8] $Gd@C_{60}[C(COOH)_2]_{10}$,[13] $Gd@C_{82}(OH)_6(NHC_2H_4SO_3H)_8$,[14] and $Gd@C_{60}(OH)_x$,[15] etc., exhibit comparable or even much higher proton relaxivities than commercial MRI contrast agents such as Gd−DTPA. Besides, the metallofullerene MRI contrast agents are expected to have low toxicity since the Gd^{3+} is well protected by the fullerene cage to avoid its release in physiological conditions. Therefore, the Gd-based EMFs would be promising materials for next generation clinical MRI contrast agents.

There are several reasons accounting for the extremely high proton relaxivity of Gd-based EMFs. First, the excellent paramagnetic properties of Gd^{3+} could largely decrease the NMR relaxation time of nearby proton nuclei of water molecules. Second, the large molecular surface of EMFs enables a large number of surrounding water molecules to interact with them. Third, as revealed by recent reports,[15−17] the aggregates of water-soluble EMFs in aqueous solution play an important role in improving the proton relaxivity of EMFs through greatly increasing their rotational correlation times.

Though EMF aggregates can enhance the magnetic resonance (MR) signals greatly, it must be pointed out that the very large EMF aggregates also have negative effects in clinical applications. Recently, MRI experiments in our laboratory found that the test mice suffered from thrombosis after injection of $Gd@C_{82}O_8(OH)_{30}$ that had been stored for long time periods, indicating the formation of large aggregates during storage. In previous studies,[15−17] two metallofullerene MRI contrast agents, i.e., $Gd@C_{60}[C(COOH)_2]_{10}$ and $Gd@C_{60}(OH)_x$, were studied with regard to their aggregates in aqueous solution as a function of concentration, temperature, pH values, and purity, etc. It was revealed that the aggregation of EMF MRI contrast agents depends on many factors, e.g., the pH values of the aqueous solution[17] and the addition of salts,[15] etc. In addition, the functional groups on the metallofullerenes also affect the EMF self-aggregation since $Gd@C_{60}[C(COOH)_2]_{10}$ and $Gd@C_{60}(OH)_x$ exhibited large differences in the size distribution of their aggregations. However, to date no time dependence for the metallofullerene MRI contrast agents has been reported.

Recently, we synthesized a new metallofullerene MRI contrast agent, $Gd@C_{82}O_6(OH)_{16}(NHCH_2CH_2COOH)_8$,[19] in which the long-chain functional groups ($-NHCH_2CH_2COOH$) and the simple hydroxy groups ($-OH$) coexist. A preliminary dynamic light scattering (DLS) study[19] indicated that this metallofullerene has a different aggregation trend from the previously reported water-soluble EMFs,[15−17] i.e., $Gd@C_{60}[C(COOH)_2]_{10}$ and $Gd@C_{60}(OH)_x$. That is, the average sizes of both $Gd@C_{60}$-

* Author to whom correspondence should be addressed. E-mail: crwang@iccas.ac.cn.
[†] Chinese Academy of Sciences.
[‡] Peking University.

10.1021/jp0615609 CCC: $33.50
Published on Web 07/15/2006

$[C(COOH)_2]_{10}$ and $Gd@C_{60}(OH)_x$ aggregates decrease monotonically along with the pH increasing from 2 to 9, whereas that of the AAD-EMF aggregates has a minimum size distribution at pH = 7. Herein, we take this molecule as a prototype to study the time dependence of metallofullerene MRI contrast agents. Various spectrometry measurements, such as DLS, scanning electron microscopy (SEM), and atomic force microscopy (AFM), were performed to study the size distribution and morphology of AAD-EMF aggregates at pH = 2, 7, and 9, respectively. The growth mechanism of EMF aggregates was proposed based on the spectrometry studies.

2. Materials and Methods

AAD-EMF were synthesized and characterized as previously described[19] and purified by chromatography using a Sephadex G-25 size-exclusion gel column with aqueous eluent at pH = 7. The sample is red-brown in aqueous solution. For investigating pH dependence of the AAD-EMF aggregations, dilute NaOH and HCl solutions were used to adjust the pH value of the AAD-EMF aqueous solutions. Finally, we prepared three samples with the same AAD-EMF concentration at 0.002 mM and different pH values at 2, 7, and 9, respectively.

DLS spectroscopy was performed to study the aggregation of both the as-prepared samples and that after 1 month of storage. The samples were introduced into several 7 mL glass bottles through a 0.45 μm filter, and the DLS measurements were carried out with a LLS spectrometer (ALV/SP-125) employing a multi-τ digital time correlator (ALV-5000) at 25.0 $\pm$ 0.5 °C. A solid-state He−Ne laser (output power of 22 mW at λ = 632.8 nm) was adopted as the light source. The data were analyzed by the CONTIN method to obtain the diffusion coefficients (D) of the solutes, and the apparent equivalent hydrodynamic radius (R_h) was determined using the Stokes−Einstein equation $R_h = kT/6\pi\eta D$, where k is the Boltzmann constant, T is the absolute temperature, and η is the solvent viscosity, respectively.

The Gd^{3+} concentrations ([Gd]) of the three samples were measured by inductively coupled plasma atomic emission spectroscopy (ICP-AES, Prodigy, Leeman, LABS, Inc.) at 342.247 nm. The proton relaxivity (R_1 in $mM^{-1}\ s^{-1}$) in aqueous solution (pH = 2, 7, and 9) was obtained by fitting the slope of $1/T_1$ versus [Gd] plots, in which T_1 was obtained by an inversion recovery pulse sequence in a Bruker Avance 600 spectrometer. The dipolar gradient was used to suppress the radiation damping effect. The T_1-weighted MR images were obtained by the spin−echo method with a 1.5 T clinical MR instrument (Sonata Siemens).

The visual morphology of AAD-EMF aggregates after 1 month of storage in aqueous solution was studied by SEM (JEOL JSM-6700F). The samples were prepared by putting a drop of the AAD-EMF solution on a wafer, and the SEM images were acquired at 15.0 kV at room temperature. The spatial structure of the AAD-EMF aggregates was further studied by AFM on a Nanoscope IIIa SPM (Digital Instruments, Santa Barbara, CA). The AFM measurements were performed in tapping mode under ambient conditions, and a hard silicon cantilever tip was used with a spring constant of 40 N/m.

3. Results and Discussions

Sitharaman et al.[17] reported that gadofullerenes such as $Gd@C_{60}(OH)_x$ and $Gd@C_{60}[C(COOH)_2]_{10}$ are pH-dependent. The proton relaxivity (R_1) of the three AAD-EMF samples after 2 days of storage in aqueous solution was measured using NMR at 600 MHz, and the measured R_1 values are 7.68, 3.83, and 2.52 $mM^{-1}\ s^{-1}$ at pH = 2, 7, and 9, respectively, so the AAD-EMF are also pH-dependent. Here it should be mentioned that the measured R_1 of AAD-EMF is similar to that of Gd−DTPA (R_1 = 3.18 $mM^{-1}\ s^{-1}$) at 600 MHz; however, because the proton relaxivity of gadofullerenes is a function of the magnetic field that shows a maximum at ca. 30−60 MHz and then falls off rapidly after 100 MHz[17] and the proton relaxivity of Gd−DTPA nearly remains constant between 30 and 600 MHz,[18] it is expected that the R_1 of the AAD-EMF would be much higher than that of Gd−DTPA at clinically relevant fields (60−100 MHz).

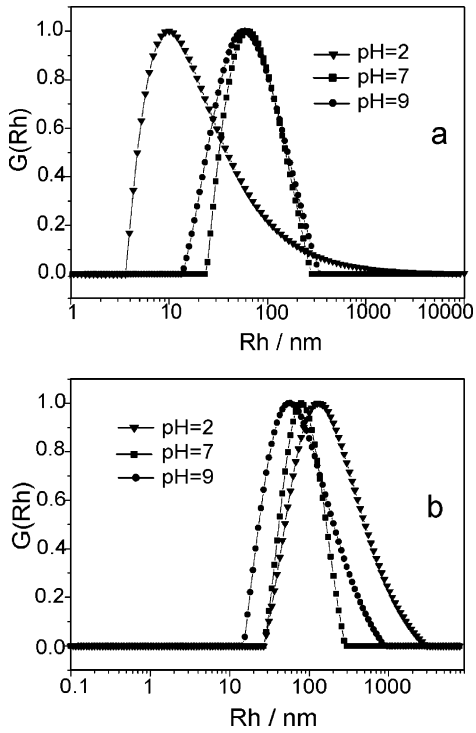

Figure 1. Size distributions of (a) the as-prepared AAD-EMF sample in aqueous solution at pH = 2, 7, and 9; (b) the same samples after 1 month of storage.

As revealed in previous studies[16,17] on $Gd@C_{60}(OH)_x$ and $Gd@C_{60}[C(COOH)_2]_{10}$, the dependence of the proton relaxivity of gadofullerene MRI contrast agents on both the applied magnetic field and the pH values of the samples is due to the aggregation of water-soluble metallofullerenes. Large gadofullerene aggregates would induce their slower tumbling/rotation in solution[17] and thus improve the proton relaxivity; therefore, it is crucial to study the aggregation behavior of AAD-EMF under different experimental conditions.

For unravelling the aggregation mechanism and the long-term stability of AAD-EMF, DLS measurements were performed at different pH values. Figures 1a and 1b exhibit the hydrodynamic radius distributions of those as-synthesized AAD-EMF samples and that after 1 month of storage in aqueous solutions, respectively. The three samples have the same AAD-EMF concentration but with different pH values at 2, 7, and 9, denoted as samples 1, 2, and 3, respectively. Obviously, sample 1 has a serious aggregation trend, since even the fresh sample in Figure 1a shows a wide size distribution from 4 to 1000 nm. After 1 month of storage, the size distribution of this sample increases to 30−3000 nm. Sample 3 also shows a marked increase in the size distribution after a long time in storage. Unexpectedly, sample 2 has an almost constant size distribution from 30 to 300 nm either before or after a long time in storage; the average hydrodynamic radius of the aggregations only increases slightly from 72.7 to 84.1 nm after 1 month of storage.

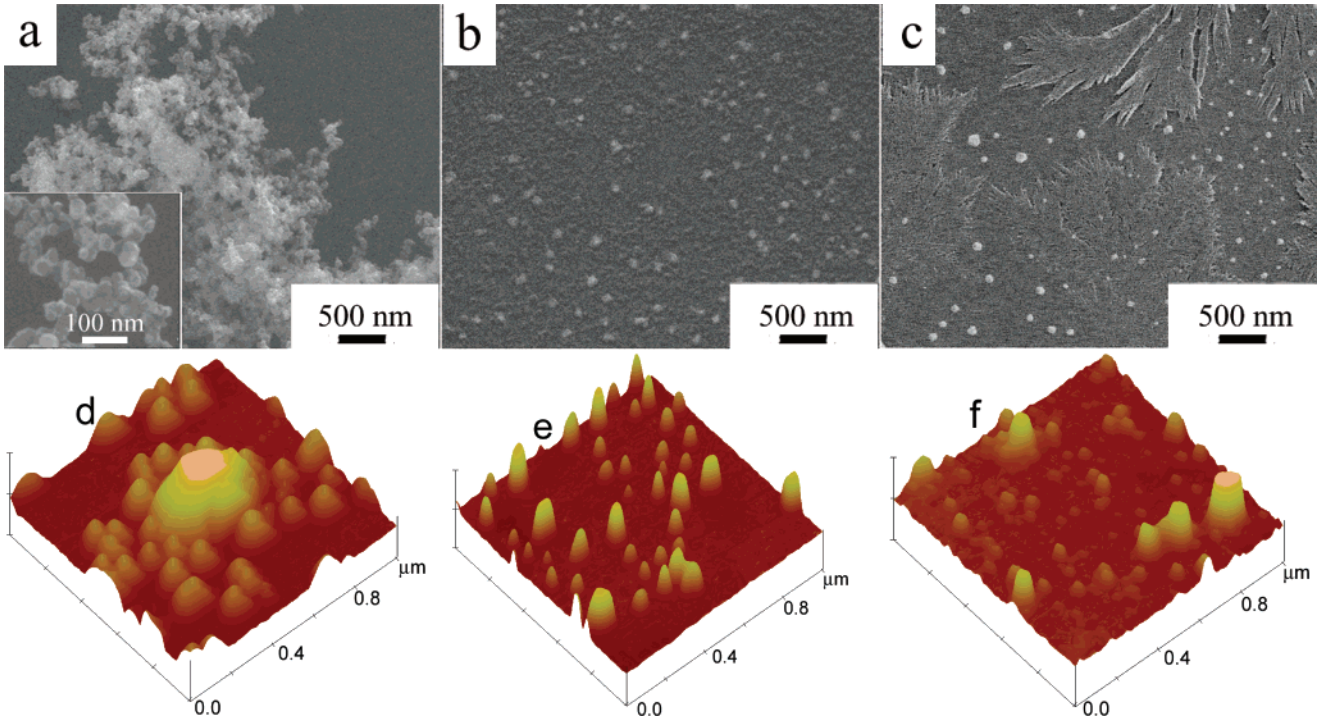

Figure 2. SEM images of AAD-EMF aggregations on wafers after 1 month of storage at different pH values in aqueous solution, (a) pH = 2, (b) pH = 7, and (c) pH = 9, and tapping-mode AFM images of same samples on a mica substrate in a 1 μm × 1 μm region, z = 15 nm, (d) pH = 2, (e) pH = 7, and (f) pH = 9. Inset in the lower left of part a is a local enlarged image of part a. The flowerlike crystals in part c are alkaline NaOH.

To further explore the self-aggregation mechanism of AAD-EMF, the visual morphology of AAD-EMF aggregates was studied by SEM. Figures 2a−c show the SEM images of the three AAD-EMF samples after 1 month of storage. A large-sized cluster network was always observed for the sample at pH = 2, and a high-resolution image (inset of Figure 2a) revealed that the large clusters are composed of many small EMF aggregates with sizes of ca. 30 nm. Whereas the aggregates at pH = 7 are some correspondingly uniform spherical particles of ca. 30−100 nm, which is in agreement with the conclusion of narrow size distribution by the DLS study. For sample 3 at pH = 9, except for the flowerlike alkaline crystals, a large size range of irregular AAD-EMF particles was observed in the image, which is also consistent with the results of the DLS measurements.

The spatial structures of the AAD-EMF aggregations were further explored by AFM. Figures 2d, 2e, and 2f are the three-dimensional AFM images of samples 1−3 after 1 month of storage, respectively. Since the experiment was performed using the same AFM tip, the broadening in lateral dimensions by tip-convolution effects[20] was not calibrated. Obviously, the AFM study reveals similar morphological characteristics of the AAD-EMF aggregations as the SEM measurements, such as the grapelike cluster network at pH = 2, correspondingly uniform nanoparticles at pH = 7, and a large size distribution of the AAD-EMF aggregations at pH = 9, and so forth.

On the basis of the geometric structure of the AAD-EMF and the morphological characteristics of AAD-EMF aggregates at different pH values, the self-aggregating mechanism of AAD-EMF was proposed. As shown in Figure 3, hydrogen-bonding effects and dipole−dipole interactions were suggested to dominate the growth of aggregates under acidic, neutral, and alkaline environments, respectively.

First, similar to other amino fullerene compounds,[21] it was supposed that the amino groups in AAD-EMF were protonated and ion-paired with Cl^- in the aqueous solution under acidic conditions at pH = 2. As shown in Figure 3, hydrogen-bonding effects induced by both the long-chain functional groups ($-N^+H_2Cl^-CH_2CH_2COOH$) and the simple hydroxyl groups ($-OH$) dominated the molecular interactions of AAD-EMF. However, as understood from the nature of the two functional groups as well as previous reports[17a] on $Gd@C_{60}[C(COOH)_2]_{10}$ and $Gd@C_{60}(OH)_x$, the hydrogen-bonding interaction induced by $-N^+H_2Cl^-CH_2CH_2COOH$ is quite weak. So along with the AAD-EMF self-aggregation driven by hydrogen-bonding interactions of both the $-N^+H_2Cl^-CH_2CH_2COOH$ and the $-OH$ groups, some of them disaggregate while the weak hydrogen bonds between $-N^+H_2Cl^-CH_2CH_2COOH/-N^+H_2Cl^-CH_2CH_2COOH$ are bombarded by solvent molecules. The concurrent aggregating and disaggregating of AAD-EMF result in a large size distribution of the EMF aggregates in a fresh sample, as shown in Figure 1a. With increasing time, however, the small particles originally formed from weak interactions between $-N^+H_2Cl^-CH_2CH_2COOH$ groups decomposed and were replaced by particles formed by the strong interactions between the $-OH$ groups. As a result, some spherical clusters with the whole surface covered by the long $-N^+H_2Cl^-CH_2CH_2COOH$ groups would be generated, and they would be hard to further merge with each other due to the steric hindrance of $-N^+H_2Cl^-CH_2CH_2COOH$. These basic unit clusters can be easily observed in Figures 2a and 2d, which represents the low-mass limit of size distribution of AAD-EMF aggregates, as shown in Figure 1b.

Second, under neutral conditions at pH = 7, proton transfers from carboxyl to amino groups often occur on some $-NHCH_2CH_2COOH$ chains to form $-N^+H_2CH_2CH_2COO^-$, then the interactions between long chains are repulsive $-N^+H_2CH_2CH_2COO^-/-N^+H_2CH_2CH_2COO^-$ but not the attractive hydrogen bonding again as that at pH = 2. In this case, the coalescence of AAD-EMF would be driven mainly by the hydrogen-

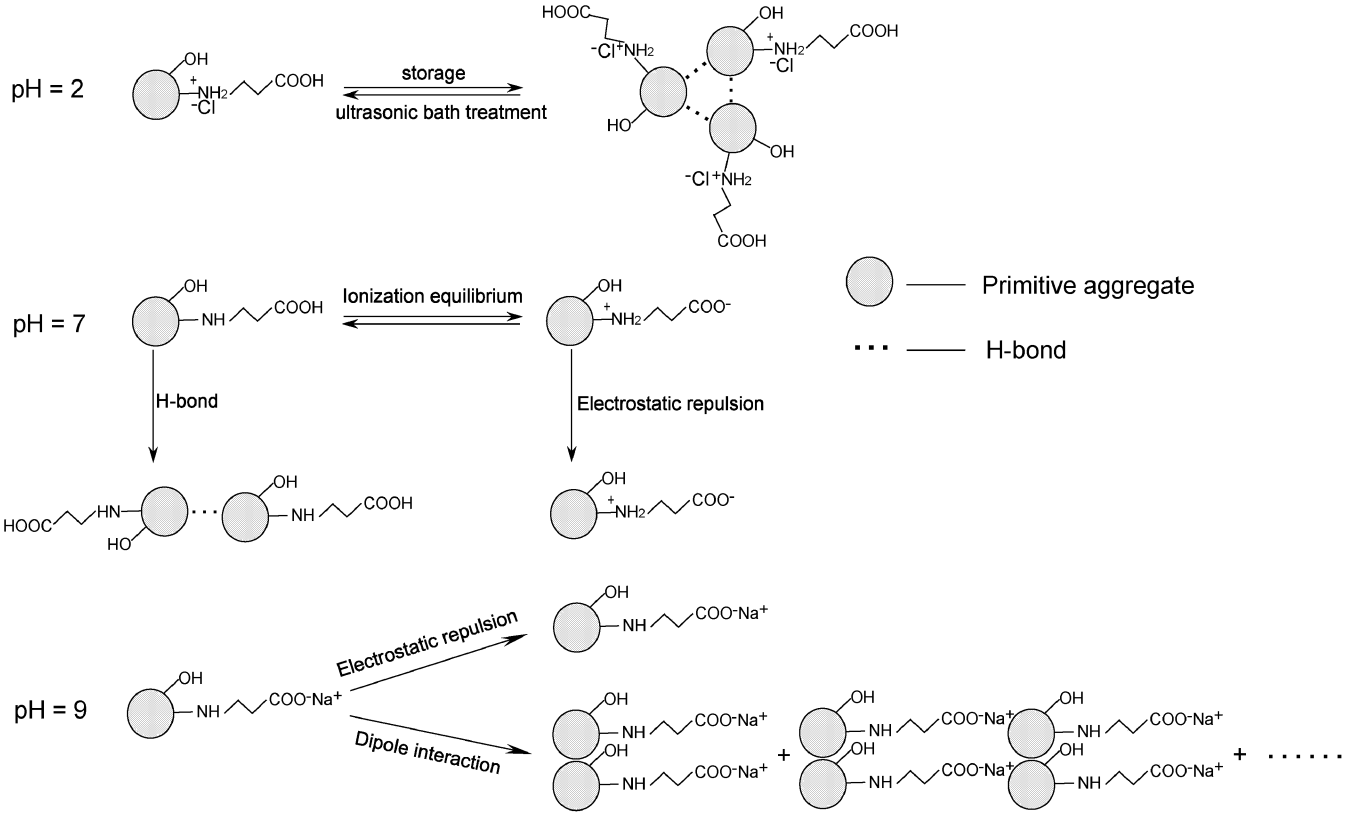

Figure 3. Suggested formation mechanism of AAD-EMF aggregations at pH = 2, 7, and 9, respectively.

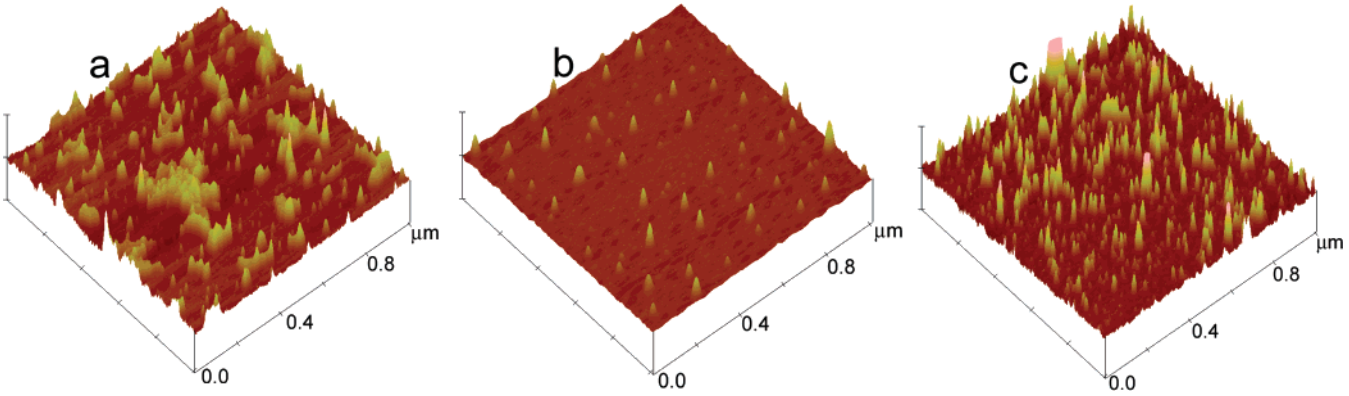

Figure 4. Tapping-mode AFM images of samples 1−3, (a) pH = 2, (b) pH = 7, and (c) pH = 9, immediately after ultrasonic treatments, in which the scanning region is 1 μm × 1 μm and z = 4 nm.

bonding interactions between hydroxyl groups. On the basis of similar analyses as that at pH = 2 for sample 1, the AAD-EMF would also self-aggregate along with increasing time to form the 30 nm size of basic unit clusters driven by the hydrogen-bonding interactions between hydroxyl groups, and the formation process is even much faster in this case due to a lack of hindrance from the aggregation/disaggregation of AAD-EMF by weak interactions between $-N^+H_2Cl^-CH_2CH_2COOH$ groups as at pH = 2. As shown in Figure 1b, both sample 1 and sample 2 exhibit the same low-mass limit of the size distribution of clusters, reflecting the formation of the same size of basic spherical clusters for them after a long time in storage. Moreover, parts of long chains on the surface of basic unit clusters in pH = 7 are in $-N^+H_2CH_2CH_2COO^-$ form, so the coalescence between clusters would be largely hindered due to their electrostatic repulsions. Figure 2e shows that only some dimers and trimers of the basic unit clusters are formed in the AFM image, which is largely different from that at pH = 2.

Third, for the alkaline environment at pH = 9, the hydrogen-bonding interactions between hydroxyl groups of the AAD-EMF are nearly inhibited by the addition of NaOH; the self-aggregation mechanism was then suggested to follow another route other than the hydrogen-bonding-dominated mechanism for sample 1 and sample 2. In view of the geometrical structure of the AAD-EMF and the morphological characteristics of aggregates revealed by SEM and AFM, a crystal-growth mechanism was proposed under this condition. As shown in Figure 3, the long chains in AAD-EMF are supposed to transform to $-NHCH_2CH_2COO^-$ under akaline conditions, and they attract Na^+ ions in aqueous solution to pair with, inducing an inhomogeneous distribution of electron density of the molecule, then the dipole−dipole interactions between AAD-EMF would induce coalescence of them to form large particles after a long time in storage.

To further understand the above self-aggregation mechanism of AAD-EMF, we put the three samples into an ultrasonic bath

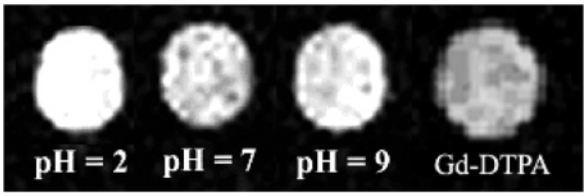

Figure 5. T_1-weighted MRI of $Gd@C_{82}O_6(OH)_{16}(NH_2CH_2CH_2COOH)_8$ (after 1 month of storage) and Gd−DTPA at the Gd concentration of 0.002 mM by the 1.5 T spin−echo method with T_R/T_E = 800 ms/15 ms, FOV = 171 × 228 mm^2, section thickness 3.0 mm, and flip angle = 90° at 24 °C.

and investigated their morphology by AFM immediately. Since neither the weak hydrogen-bonding interaction nor the dipole−dipole interaction between AAD-EMF can tolerate the powerful ultrasonic treatment, the AFM images obtained by this time reflect the morphology of the AAD-EMF aggregates at the very preliminary stage. As shown in Figure 4a, a huge cluster network was formed quickly at pH = 2, revealing very large driving forces of the hydrogen-bonding effect in this case. At pH = 7, some uniform clusters were observed to isolate from each other (Figure 4b), confirming the repulsive nature of EMF clusters due to the repulsive interactions between $-N^+H_2CH_2CH_2COO^-$. Whereas at pH = 9 (Figure 4c), the AAD-EMF neither form a cluster network as that in sample 1 nor form isolated uniform clusters as that in sample 2, so the self-aggregation mechanism must be different from that of sample 1 and sample 2 under this condition.

Finally, in vitro MRI studies for the three samples and Gd−DTPA were performed for comparison, and the results are shown in Figure 5. It was observed that the relative intensity of MR signals for sample 1 (pH = 2; relative intensity, 121.5) is the largest, that for sample 3 (pH = 9; relative intensity, 110.0) the second, and that for sample 2 (pH = 7; relative intensity, 107.5) the last. The sequence of signal intensity for the three samples is consistent with the order of their size distributions; that is, sample 1 aggregates the most, sample 3 the second, and sample 2 the third. Though the efficiency of the MR signal enhancement for sample 2 is somewhat lower than that of samples 1 and 3, it is still higher than that of Gd−DTPA (105.3), indicating the potential of AAD-EMF as highly efficient next generation MRI contrast agents.

4. Conclusion

In conclusion, under acidic conditions, the self-aggregation of the newly synthesized AAD-EMF is dominated by hydrogen-bonding effects. The small substable nanoclusters of ∼30 nm in size are first formed, and these small nanoclusters subsequently self-assemble to form a large cluster network. Under neutral conditions (pH = 7), the self-aggregation of AAD-EMF is also dominated by the hydrogen-bonding effect, leading to the formation of similar substable nanoclusters as those formed at pH = 2. However, at pH = 7, the repulsive charged $-N^+H_2CH_2CH_2COO^-$ groups on the surfaces of the substable nanoclusters largely inhibit their further coalescence, so a narrow size distribution of AAD-EMF aggregations is obtained. In contrast, the self-aggregation of AAD-EMF under alkaline conditions followed a crystal-growth mechanism, resulting in the formation of large and rigid particles after long time storage in aqueous solution. The high proton relaxivity and narrow size distribution of AAD-EMF under neutral conditions provide a great potential for developing novel EMF next generation MRI contrast agents.

Acknowledgment. C.R.W. thanks the National Science Foundation of China (Grant Nos. 50225206, 90206045, and 20121301), the Major State Basic Research Program of China "Fundamental Investigation on Micro−Nano Sensors and Systems based on BNI Fusion" (Grant No. 2006CB300402), and the National Center for Nanoscience and Technology of China.

References and Notes

(1) (a) Chai, Y.; Guo, T.; Jin, C.; Haufler, R. E.; Chibante, L. P. F.; Fure, J.; Wang, L.; Alford, J. M.; Smalley, R. E. *J. Chem. Phys.* **1991**, *95* (20), 7564. (b) Shinohara, H. *Rep. Prog. Phys.* **2000**, *63*, 843.

(2) Hasegawa, Y.; Ling, Y.; Yamazaki, S.; Hashizume, T.; Shinohara, H.; Sakai, A.; Pickering, H. W.; Sakurai, T. *Phys. Rev. B* **1997**, *56*, 6470.

(3) Chen, C.; Xing, G.; Wang, J.; Zhao, Y.; Li, B.; Tang, J.; Jia, G.; Wang, T.; Sun, J.; Xing, L.; Yuan, H.; Gao, Y.; Meng, H.; Chen, Z.; Zhao, F.; Chai, Z.; Fang X. *Nano Lett.* **2005**, *5*, 2050.

(4) Cagle, D. W.; Kennel, S. J.; Mirzadeh, S.; Alford, J. M.; Wilson, L. J. *Proc. Natl. Acad. Sci. U.S.A.* **1999**, *96*, 5182.

(5) Wilson, L. J.; Cagle, D. W.; Thrash, T. P.; Kennel, S. J.; Mirzadeh, S.; Alford, J. M.; Ehrhardt, G. J. *Coord. Chem. Rev.* **1999**, *190*, 199.

(6) Lezzi, E. B.; Duchamp, J. C.; Fletcher, K. R.; Glass, T. E.; Dorn, H. C. *Nano Lett.* **2002**, *2*, 1187.

(7) Wilson, L. J. *Electrochem. Soc. Interface* **1999**, (Winter), 24.

(8) Mikawa, M.; Kato, H.; Okumura, M.; Narazaki, M.; Kanazawa, Y.; Miwa, N.; Shinohara, H. *Bioconjugate Chem.* **2001**, *12*, 510.

(9) Kato, H.; Kanazawa, Y.; Okumura, M.; Taninaka, A.; Yokawa, T.; Shinohara, H. *J. Am. Chem. Soc.* **2003**, *125*, 4391.

(10) Lauffer, R. B. *Chem. Rev.* **1987**, *87*, 901.

(11) Caravan, P.; Ellison, J. J.; McMurry, T. J.; Lauffer, R. B. *Chem. Rev.* **1999**, *99*, 2293.

(12) Senapati, L.; Schrier, J.; Whaley K. B. *Nano Lett.* **2004**, *4*, 2073.

(13) Bolskar, R. D.; Benedetto, A. F.; Husebo, L. O.; Price, R. E.; Jackson, E. F.; Wallace, S.; Wilson, L. J.; Alford, J. M. *J. Am. Chem. Soc.* **2003**, *125*, 5471.

(14) Lu, X.; Xu, J. X.; Shi, Z. J.; Sun, B. Y.; Gu, Z. N.; Liu, H. D.; Han, H. B. *Chem. J. Chin. Univ.* **2004**, *25* (4), 697−700.

(15) Laus, S.; Sitharaman, B.; Tóth, E.; Bolskar, R. D.; Helm, L.; Asokan, S.; Wong, M. S.; Wilson, L. J.; Merbach, A. E. *J. Am. Chem. Soc.* **2005**, *127*, 9368.

(16) Sitharaman, B.; Asokan, S.; Rusakova, I.; Wong, M. S.; Wilson, L. J. *Nano. Lett.* **2004**, *4*, 1759.

(17) (a) Sitharaman, B.; Bolskar, R. D.; Rusakova, I.; Wilson, L. J. *Nano Lett.* **2004**, *4*, 2373. (b) Toth, E.; Bolskar, R. D.; Borel, A.; González, G.; Helm, L.; Merbach, A. E.; Sitharaman, B.; Wilson, L. J. *J. Am. Chem. Soc.* **2005**, *127*, 799.

(18) (a) Shukla, R. B.; Kumar, K.; Weber, R.; Zhang, X.; Tweedle, M. *Acta Radiol.* **1997**, *38*, 121. (b) Aime, S.; Botta, M.; Panero, M.; Grandi, M.; Uggeri, F. *Magn. Reson. Chem.* **1991**, *29*, 923. (c) Merbach, A. E.; Toth, E. *The Chemistry of Contrast Agents in Medical Magnetic Resonance Imaging*; John Wiley and Sons: New York, 2001.

(19) Shu, C.-Y.; Gan, L.-H.; Wang, C.-R.; Pei X.-L.; Han H.-B. *Carbon* **2006**, *44*, 496.

(20) Samori, P.; Francke, V.; Mangel, T.; Mullen, K.; Rabe, J. *Opt. Mater.* **1998**, *9*, 390.

(21) Richardson, C. F.; Schuster, D. I.; Wilson, S. R. *Org. Lett.* **2000**, *2* (8), 1011.